Sheath parameters for non-Debye plasmas: simulations and arc damage

I. Morozov, G. Norman
Joint Institute of High Temperatures of RAS, Moscow, Russia

Z. Insepov, J. Norem*
*Argonne National Laboratory, Argonne, IL 60439, USA**

(Dated: September 29, 2011)

In this paper we report results for MD simulations of the dense, nonideal plasma sheath near a metallic surface. We use Molecular Dynamics (MD) to evaluate sheaths in the non-Debye region for high density, low temperature plasmas. We use direct two-component MD simulations where the interactions between all electrons and ions are computed explicitly. Although MD simulations have limited space and time scales their results can be considered as the lower level output for the multiscale approach. We find that the non-Debye sheath can be extrapolated from the Debye sheath parameters with small corrections. Using these results, and equating surface tension and plasma pressure, it is possible to infer a range of plasma densities and sheath potentials from SEM images of arc damage. We find that these parameters are consistent with previous PIC code estimates, pointing to densities in the range 10^{24} - $10^{25}/\mathrm{m}^3$. The sub-micron component of arc damage can be both: a) the most direct indicator the internal parameters of the arc plasma, and b) the most likely cause of further breakdown events due to high enhancement factors.

I. INTRODUCTION

Vacuum arcs are involved in many fields, from high power switching, surface coating and a variety of laboratory and commercial applications, and these arcs have been under study for many years. The properties of these dense, non-Debye plasmas, however, are not well understood in spite of the fact that these plasmas seem to limit the performance of both major accelerator and tokamak facilities and the general behavior of these arcs has been known since 1901 [1]. In part, the reason for this situation is that experimentally the arcs are very small, develop very fast and are hard to measure. Theory and modeling are complicated by the large number of mechanisms that seem to be involved in arcs evolution, so that it is difficult to identify and measure enough data to constrain the models. While arc damage has been measured and catalogued for over a hundred years, there has not been any clear correspondence between components of the arc damage and the past or subsequent behavior of the arc. We argue in this paper that the dominant components of arc damage are due to the high density, high sheath potential plasma that produces a high plasma pressure, producing very small structures, at or below scale lengths of a few hundred nm. These structures may or may not survive the subsequent cool-down of the liquid surface, however the cool down itself also seems to produce cracks with small structures [2–5] .

Our basic assumptions are that the development of the arc can be explained by two mechanisms: 1) mechanical failure of the solid surface due to Coulomb explosions caused by high surface fields, and, 2) the development of unipolar arcs. The PIC simulations in the framework of the unipolar arc model for rf cavity breakdown [2–5] show that the density of plasma formed above the field emitting asperities can be as high as $10^{26}\mathrm{m}^{-3}$. The temperature of such plasma is in the range of $1-10$ eV. These extreme conditions lead the Debye screening length $\lambda_D = \sqrt{\epsilon_0 k_B T/n_e e^2}$ to become smaller than the mean interparticle distance or the formal number of particles in the Debye sphere $N_D = 4\pi n_e \lambda_D^3/3$ to become less that unity. It implies the failure of the ideal plasma approximation. Most of the processes in such a dense plasma are governed by particle collisions so that the PIC method which relies on a rough collisional model becomes inappropriate, as shown in Fig 1.

For this purpose we use direct two-component MD simulations where the interactions between all electrons and ions are computed explicitly. Although MD simulations have limited space and time scales their results can be considered as the lower level output for the multiscale approach.

Equilibrium and non-equilibrium nonideal plasmas have been studied extensively by MD in the past several decades [6–10]. Nevertheless there are few studies of the spatially inhomogeneous systems such as electric double layers or plasma sheath. In this paper we report on the first results for MD simulations of the nonideal plasma sheath near a metallic surface.

*Electronic address: norem@anl.gov

The estimates of the surface fields, combined with plasma density give estimates of the plasma pressure that can be compared with experimental data. It is possible to make experimental estimates of the plasma pressure by comparing the linear dimensions of structures seen in the surface with estimates obtained from comparing the surface tension of the liquid metal with the plasma properties. We describe how the scale of structures frozen in to metal as the arc cools can be used to set limits on the plasma properties.

II. SIMULATION TECHNIQUE

The two-component fully ionized electron-ion plasma is considered. Neutral atoms are not taken into account which can affect relaxation times at relatively low plasma densities when the density of neutrals is high enough. It should not, however, affect the stationary distribution of charges. In the present work the simulations are restricted to the singly ionized plasma with $Z = 1$.

The electron-electron and ion-ion interactions are given by the Coulomb potential. For electrons and ions it is modified at short distances to account for quantum effects. The equation below assumes a Gaussian wave function for an electron

$$V_{ei}(r) = \frac{Ze^2}{4\pi\epsilon_0 r}\mathrm{erf}\left(\frac{r}{r_0}\right), \tag{1}$$

where the r_0 parameter that equals to 0.21 nm in out case to match the ionization energy for copper at $r = 0$: $U(0) = -7.73$ eV (see Fig. 2). The similar interaction model was used e.g. in [10–12] for simulations of ionized metallic clusters. More accurate electron-ion and electron-electron interaction models are discussed e.g. in [13, 14] although they seem to be redundant for this particular case. In fact the results are weakly dependent on the short distance part of the potential as the change of the $U(0)$ value from 7.73 eV to 5.1 eV does not change the results within simulation accuracy.

The velocity Verlet algorithm is applied to solve the classical equations of motion for electrons and ions. The method takes into account the conservation of the total energy of the finite system, as long as there is no external potential. To follow the electron dynamics, time steps of $0.001 - 0.01$ fs were taken to calculate the time evolution.

The general simulation scheme follows the method described in [15] and shown in Fig. 3. First an equilibrium MD trajectory is calculated for the system at given density and temperature using the nearest image method (periodic boundary conditions) for all dimensions. The simulation box size and other parameters are summarized in Table I. The Langevin thermostat is used initially to brought system to an equilibrium state while it is switched off for a production run. Then the system becomes adiabatic which ensures that all thermodynamic quantities are conserved in average. The ion mass is set to be equal to the electron mass for better mixing of ionic trajectories at this phase.

T, eV	$n_e, 10^{27}\mathrm{m}^{-3}$	L_x, nm	L_z, nm	N_i	Γ	Θ	λ_D, nm
1	0.0001	120	360	518	0.11	0.001	23.5
1	0.001	55	165	499	0.23	0.004	7.43
1	0.01	25	75	468	0.50	0.017	2.35
1	0.1	11	33	399	1.08	0.079	0.74
1	1.0	5	15	375	2.32	0.36	0.24
1	5.0	2.8	8.4	329	3.97	1.07	0.11
10	0.01	25	75	468	0.05	0.002	7.43
10	1.0	5	15	375	0.23	0.036	0.74
10	100	1	2.5	300	1.08	0.79	0.07

TABLE I: MD simulation parameters: T is the initial electron temperature, n_e is the initial number density of electrons (or ions), L_z is the transversal simulation box size, L_x is the longitudinal simulation box size, N_i is the number of ions which is equal to the initial number of electrons, $\Gamma = e^2(4\pi n_e/3)^{1/3}/(4\pi\epsilon_0 k_B T)$ is the nonideality parameter, $\Theta = \hbar^2(3\pi^2 n_e)^{2/3}/(2m_e k_B T)$ is the degeneracy parameter, λ_D is the Debye length.

At the second phase the particle positions and velocities at particular time moments are taken from the equilibrium trajectory to be used as the initial states for nonequilibrium simulations of the plasma sheath. The interval between those points should be large enough for the initial states to be statistically independent from the microscopical point of view. However, all these states correspond to the same macroscopical conditions as they are taken from a single equilibrium trajectory. Then a bunch of trajectories is computed starting from the given ensemble of initial states and the results are averaged over the ensemble.

In order to study the plasma sheath, the XY plane at $z = 0$ axis is considered as a metallic surface whereas a reflecting wall is introduced on the other side of the box at $z = L_z$. The periodic boundary conditions are still applied for transverse dimensions x and y. When an electron crosses the surface it is always meant to be absorbed. Therefore it is removed from the system and the overall surface charge is incremented by its charge $q_{\rm surf} \leftarrow q_{\rm surf} - e$.

A non-zero surface charge produces an electrostatic field which influence the particles. As the system has a finite size on the transverse dimensions the electrostatic potential caused by the surface at a distance z is given by

$$\phi(z) = \frac{\sigma}{4\pi\epsilon_0} \int\limits_{-L_x/2}^{L_x/2} dx \int\limits_{-L_y/2}^{L_y/2} dy \, \frac{1}{\sqrt{x^2+y^2+z^2}}\,, \tag{2}$$

where $\sigma = q_{\rm surf}/(L_x L_y)$ is the surface charge density and L_x, L_y are the box sizes in the transverse dimensions. The integration should be performed from $-L_\alpha/2$ to $L_\alpha/2$ for all particles in accordance with the nearest image approach. Assuming $L_x = L_y = 2a$ one can obtain

$$\phi(z) = -\frac{\sigma}{\pi\epsilon_0}\left(z \arctan\left[\frac{a^2}{z\sqrt{2a^2+z^2}}\right] + a \log\left[\frac{\sqrt{2a^2+z^2}-a}{\sqrt{2a^2+z^2}+a}\right]\right), \tag{3}$$

$$E_z(z) = -\frac{\partial\phi}{\partial z} = \frac{\sigma}{\pi\epsilon_0} \arctan\left[\frac{a^2}{z\sqrt{2a^2+z^2}}\right], \tag{4}$$

where E_z is the longitudinal component of the electric field. It can be shown that Eq. (4) tends to the infinite surface field expression $E_z = \sigma/(2\epsilon_0)$ as $z \to 0$ and to the Coulomb filed $E_z = \sigma a^2/(\pi\epsilon_0)/z$ as $z \to \infty$. It is important to use Eq. (4) in the simulation with the given boundaries instead of the infinite surface field $E_z = \sigma/(2\epsilon_0)$ as the later cannot be screened by plasma particles at a large distance. As the surface field grows it starts to repel electrons from surface until the stationary state is reached.

We do not compute dynamics of ions at this phase as the ions are too heavy to contribute to the simulation results at the electron time scale. At the same time the ions are movable at the equilibrium trajectory that is used for generation of the initial states. Thus the averaging over an ensemble means the averaging over different configurations of ions.

It was checked that the final results are independent of the simulation box size. If the box is doubled the deviation of the results are in within the statistical errors.

The thermodynamics parameters was maintained in the course of simulation. It was found that the overall electron temperature deviates in the range of $1 - 10\%$ due to absorption of the most energetic electrons to the surface.

III. FITTING RESULTS

Typically the relaxation of the electric field is observed for about 1 ps (see Fig. 4). The development of the electron profile is shown in Fig. 5. The stationary density profiles obtained after the relaxation are shown in Fig. 6. As the ions does not move, their distribution mimics the uniform distribution obtained from the equilibrium trajectory with full periodic boundary conditions. On the contrary, electrons form the well pronounced layer of plasma near the surface with a positive charge which we consider as the plasma sheath.

The plasma charge density profile is given by the difference between the ion and electron densities as presented in Fig. 7 in the semilogarithmic scale. It is seen that starting from the surface the charge density $\sigma(z)$ decays exponentially which agrees with the Debye approximation. At high densities, however, the exponential decay is preceded by a non-exponential area due to the plasma nonideality. This regions makes difference between calculation of the sheath length from the slope $\lambda_{\rm exp}$ of the exponential decay $\sigma(z) \sim {\rm e}^{-z/\lambda_{\rm exp}}$ and from the distance λ at which the charge density decreases at the value of ${\rm e} = 2.71$ ($\sigma(\lambda) = \sigma(0)/{\rm e}$) as illustrated in Fig. 7c.

Both quantities $\lambda_{\rm exp}$ and λ are presented in Fig. 8 depending on the plasma density and temperature. It is seen that $\lambda_{\rm exp}$ follows the Debye-like dependence on density $\lambda_{\rm exp} \sim n_e^{-1/2}$ whereas the real sheath length λ scales with a slightly different exponent.

The fits for MD data are

$$T_e = 1{\rm eV}: \qquad \lambda_{\rm exp} = 1.7\lambda_D, \quad \lambda[{\rm nm}] = 1.0 \cdot 10^{11} (n_e[m^{-3}])^{-0.405}, \tag{5}$$

$$T_e = 10{\rm eV}: \qquad \lambda_{\rm exp} = 1.7\lambda_D, \quad \lambda[{\rm nm}] = 3.18 \cdot 10^{12} (n_e[m^{-3}])^{-0.449}. \tag{6}$$

Fig. 9 shows the ratios $\lambda_{\rm exp}/\lambda_D$ and λ/λ_D depending on both electron density and nonideality parameter. It is seen from Fig. 9b that the values of λ/λ_D for different temperatures are close to each other when plotted versus the parameter Γ. It confirms the idea that the difference between λ and λ_D is related to the plasma nonideality.

The values of the electric field at the metal surface are presented in Fig. 10 depending on both temperature and density. The solid line corresponds to Eq. (2) from [16]

$$E = \frac{V_f}{\lambda_D} = [n_e k_B T_e/(4\epsilon_0)]^{1/2} \log[M_i/(2\pi m_e)], \tag{7}$$

where M_i and m_e are the masses of electron and ion. If the Debye radius in Eq. (7) is substituted by the MD result (5) or (6) it results in the values shown by crosses in Fig. 10 which are in a better agreement with the MD results.

The fits for MD data shown by dashed lines are

$$T_e = 1\text{eV}: \qquad E[\text{GV/m}] = 2.57 \cdot 10^{-15} (n_e[m^{-3}])^{-0.577}, \tag{8}$$

$$T_e = 10\text{eV}: \qquad E[\text{GV/m}] = 1.21 \cdot 10^{-13} (n_e[m^{-3}])^{-0.531}. \tag{9}$$

Fig. 11 shown the plasma potential calculated using the simple relation of $\phi = E/\lambda$ where both the surface electric field E and the sheath length λ are obtained from MD simulations. A more rigorous result can be found by integration of the electric field distribution in plasma but it requires a more accurate evaluation of the space charge away from the sheath area and will be the subject of future work.

IV. EXPERIMENTAL ESTIMATES OF PLASMA PARAMETERS

The plasma pressure is defined by,

$$p = nk(T + \phi) - \epsilon_0 E^2/2, \tag{10}$$

which, in the limit of small E and T is a function primarily of the sheath potential, $\phi \sim 5T_e$. If the pressure is unevenly applied, it will produce a deformation in a liquid surface that is opposed by surface tension, see Fig 12. The approximate scale of these effects is set by the equilibrium radius, r, where the surface tension is balanced by the plasma pressure can obtained by equating the surface tension force around the circumference with the pressure over the whole area [17],

$$2\pi r\gamma = \pi r^2 p, \tag{11}$$

with γ equal to the surface tension constant, approximately 1 N/m, giving $r \sim 2\gamma/p$ [18]. For small structures it has been shown by Tolman that this expression should be corrected by a factor δ, using the expression,

$$r = \frac{2\gamma}{p}\left(1 - \frac{\delta}{r} + \cdots\right), \tag{12}$$

where δ is the Tolman length [19]. The Tolman length is generally evaluated using Molecular Dynamics, and estimates vary from tenths of molecular dimensions to hundredths of atomic dimensions. For radii, r, on the order of 100 nm this correction is not significant.

There are many types of arc damage that have been seen SEM images [20]. The damage from a single event is generally circular, in the range of 5 - 200 μm in diameter, and frequently craterlike with a raised rim. The damage usually shows signs of melting. If the surface has absorbed significant energy it is reasonable to assume that fine structure from the arc is lost as the metal solidifies, If the arc deposits little energy to the surface, for example in SEM images of damage, Fig 14, a) from 201 MHz rf coupler, and b) from arc damage from Castano [21] and images from laser damage [16], we find complex structures on the scale of 100 - 300 nm, which are not seen in arc damage where large amounts of energy ($\sim$1 J) were present. We assume that if large amounts of energy are transmitted through an arc crater there is less small scale structure, consistent with high stored heat keeping the metal liquid until the surface tension smoothed off the surface. We find that classic unipolar arc tracks (where magnetic fields move the arc in rapid retrograde motion) are associated with more fine structure, consistent with faster liquid cool down preserving this fine structure.

Simulations of unipolar arcs using PIC codes [5] have shown that the plasma potential seems to stay approximately 50 to 75 V during the development of the arc, thus the variation in plasma pressure is primarily due to the plasma ion density. Schwirzke showed that unipolar arcs could produce holes 5 times deeper than their diameter (0.7 μm) [16]. If we assume that these structures grew from craters with $r \leq 0.2$ - 0.35 μm, and the plasma potential, ϕ was 50 V, this would imply that the density of the plasma had to be at least $1 - 4 \times 10^{24}$ m^{-3}, see Fig 13. This is consistent with estimates made from the PIC code, which would not be expected to be reliable at these high densities.

The primary arc damage that results in further high enhancement factors and further breakdown events is likely due to this sub-micron damage, coming either from the plasma pressure itself producing a turbulent surface if it can quickly cool, or cracks produced when the large molten area beneath the arcs cools from the melting point of copper to room temperature leaving a network of surface cracks. The production of high enhancement factors in surface cracks has been demonstrated in Ref [3, 4]. The sub-micron component of arc damage thus appears to be both the most direct indicator of the internal parameters of the arc plasma, and the most likely to produce further breakdown events due to high enhancement factors.

V. CONCLUSIONS

The classical molecular dynamics simulations were performed to study the nonideal plasma sheath at a metal surface for the conditions appropriate to those found in accelerator cavities. The simulations started from the uniform equilibrium plasma state. Then the relaxation of the electron density profile with formation of the plasma sheath was observed. The relaxation time was found to be of the order of ~ 100 fs. It was shown that the plasma sheath length depends on the electron number density in a slightly different way than the usual expression for the Debye radius due to a non-exponential charge profile at short distances. The values of the sheath length and the surface field were obtained for two values of temperatures and a wide density range with the nonideality parameter $\Gamma = 0.1 - 4$. We compare the MD results with the contemporary theoretical models and with experimental data from damage. When we compare the plasma conditions that would result from these sheaths with data we find damage consistent with the high plasma pressures implied by the MD and PIC results. We find that the high density plasma these results imply and the level of plasma pressure it would produce is consistent with the scale of arc damage, in examples where the arc would cool before this structure would be lost. This implies that the sub-micron component of arc damage is be both the most direct indicator of the internal parameters of the arc plasma, and, in the case of cracks, the most likely to produce further breakdown events due to high enhancement factors.

VI. ACKNOWLEDGEMENTS

We thank the staff of the Accelerator and Technical Divisions at Fermilab and the Muon Accelerator Program (MAP) for supporting and maintaining the MAP experimental program in the MTA experimental area. The work at Argonne is supported by the U.S. Department of Energy Office of High Energy Physics under Contract No. DE-AC02-06CH11357.

[1] R. F. Earhart, Phil. Mag. **1,** 147 (1901).
[2] Z. Insepov, J. Norem, D. Huang, S. Mahalingam, S. Veitzer, Proceedings of PAC09, Vancouver, B. C., Canada, May 4-8, (2009) 800.
[3] Z. Insepov, J. Norem, T. Proslier, S. Mahalingam, S. Veitzer, Proceedings of LINAC10, Tsukuba Japan, Sept 12-17, (2010) 205.
[4] Z. Insepov, J. Norem, S. Veitzer, S. Mahalingam, Proceedings of RF2011, June 1-3, Newport R. I. (to be published), arXiv:1108.0861.
[5] Z. Insepov, J. Norem, Th. Proslier, A. Moretti D. Huang, S. Mahalingam, S. Veitzer; arXiv:1003.1736v3 (2010).
[6] T. Pschiwul, G. Zwicknagel; J. Phys. A, **36**, 6251 (2003).
[7] I.V. Morozov, G.E. Norman; JETP, **100**, 370 (2005).
[8] L.X. Benedict, J.N. Glosli, D.F. Richards, F.H. Streitz, P. Hau-Riege, R.A. London, F.R. Graziani, M.S. Murillo, J.F. Benage; Phys. Rev. Lett. **102**, 205004 (2009).
[9] Z. Donko; J. Phys. A, **42**, 214029 (2009).
[10] T. Raitza, H. Reinholz, G. Röpke, I. Morozov, E. Suraud; Contrib. Plasma Phys. **49**, 498 (2009).
[11] M. Belkacem, F. Megi, P.-G. Reinhard, E. Suraud, and G. Zwicknagel; Eur. Phys. J. D **40**, 247 (2006).
[12] G. Zwicknagel, T. Pschiwul; Contrib. Plasma Phys. **43**, 393 (2003).
[13] A.V. Filinov, M. Bonitz, W. Ebeling; J. Phys. A **36**, 5957 (2003).
[14] I.V. Morozov, I.A. Valuev; J. Phys. A, **42**, 214044 (2009).
[15] A.Y. Kuksin, I.V. Morozov, G.E. Norman, V.V. Stegailov, I.A. Valuev; Mol. Simulat. **31**, 1005 (2005).
[16] F.R. Schwirzke; IEEE T. Plasma Sci. **19**, No. 5, 690 (1991).
[17] J. He, N. M. Miskovsky, P. H. Cutler and M. Chung, J. Appl. Phys. **68(4)**, (1990) 1475.
[18] T. Matsumoto, H. Fujii, T. Ueda, M. Kamai and K. Nogi, Meas. Sci. Technol. **16**, (2005) 432.
[19] R. C. Tolman, J. Chem. Phys. **17**, 333 (1949).

[20] A. Anders, *Cathodic Arcs, From Fractal Spots to Energetic Condensation*, Springer, New York (2008), Chapter 3.
[21] C. H. Castano G., presented at "Workshop on Unipolar Arcs", Argonne, Jan. 29 (2010), https://twindico.hep.anl.gov/indico/conferenceDisplay.py?confId=69

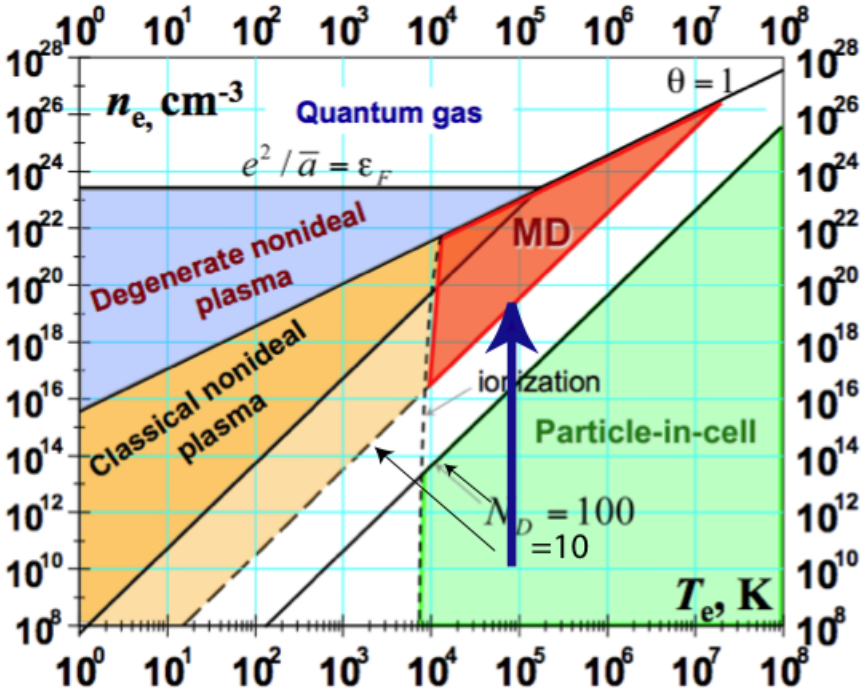

FIG. 1: The range of PIC and MD codes. The arrow shows the time development on an arc, as described in ref [2–5]

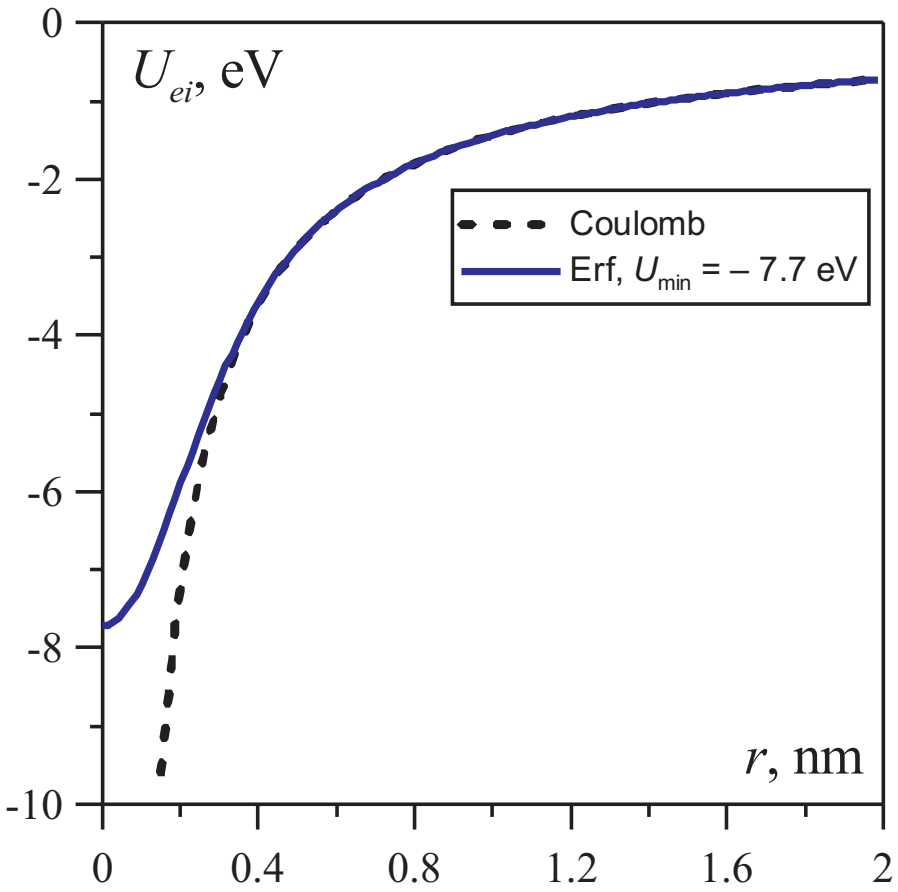

FIG. 2: Electron-ion interaction potential: dashed line – pure Coulomb, solid line – the one used in this work.

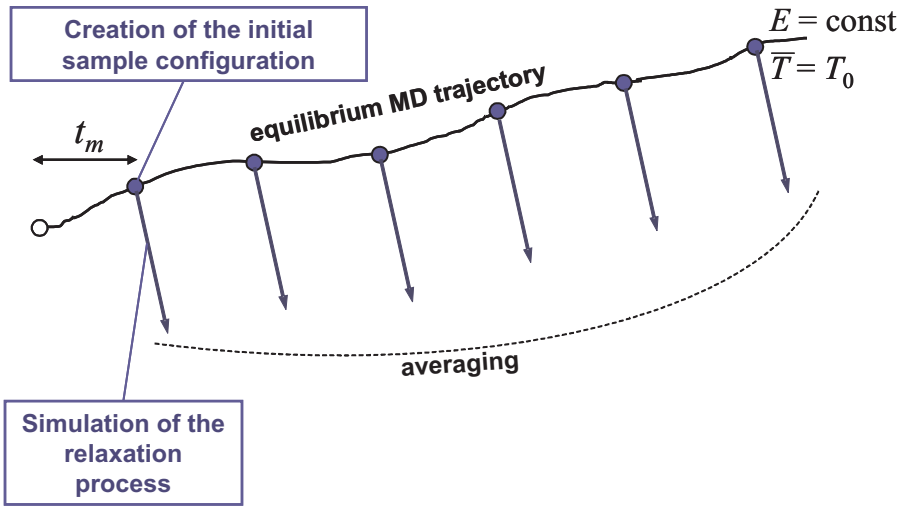

FIG. 3: General simulation scheme: averaging over an ensemble of initial states taken from an auxiliary equilibrium trajectory (solid curve with points).

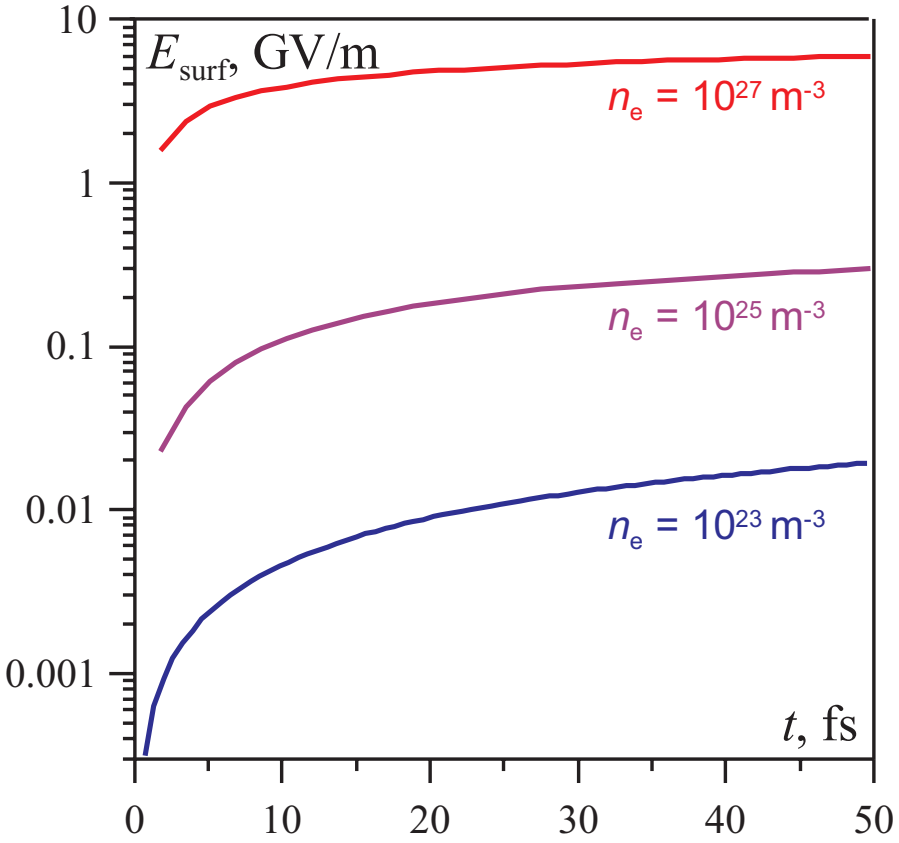

FIG. 4: Dependence of the electric field strength at the surface on time for different electron number densities (shown on the plot); $T = 1$eV.

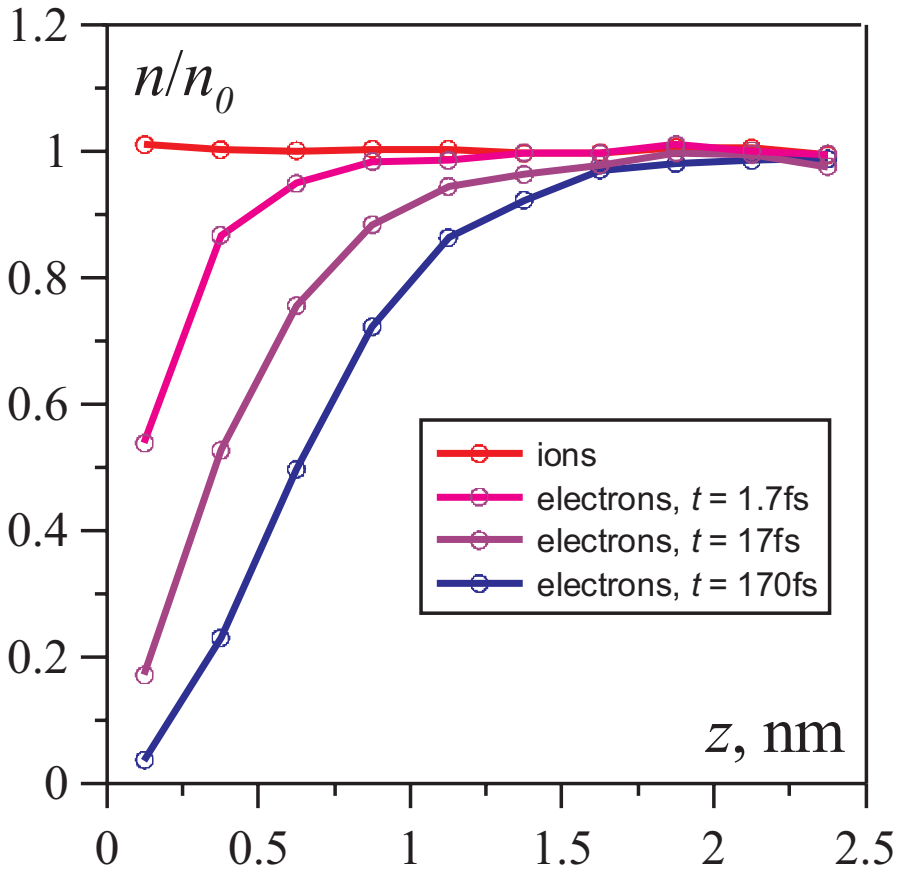

FIG. 5: Development of the electron density profile with time. The time moments are shown in the legend. The density is normalized by the mean density in the initial state; $n_e = 10^{23}\mathrm{m}^{-3}$, $T = 1\mathrm{eV}$.

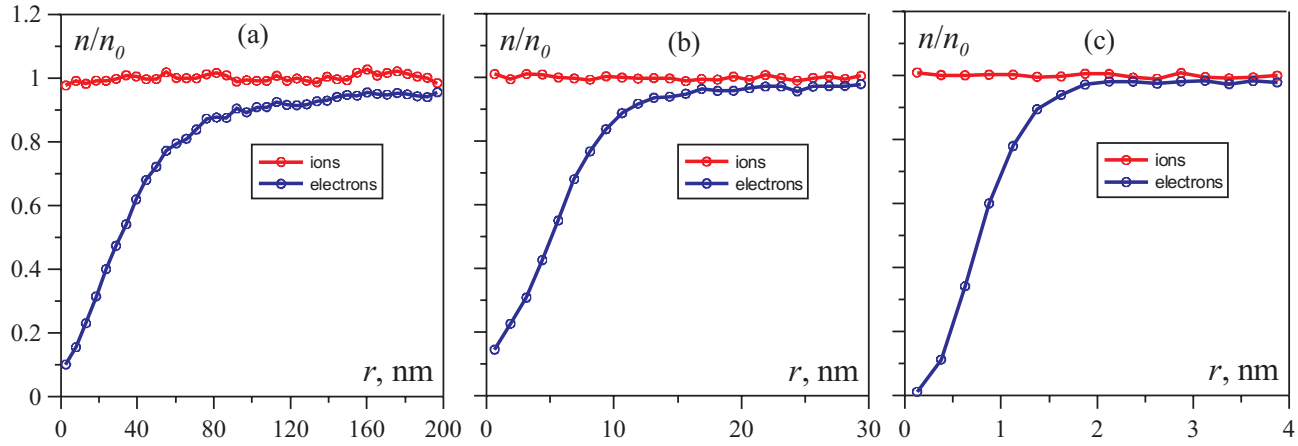

FIG. 6: Density profiles for electrons and ions at the final stationary state depending on the mean electron number density: (a) $n_e = 10^{23}\mathrm{m}^{-3}$ (b) $n_e = 10^{25}\mathrm{m}^{-3}$, (c) $n_e = 10^{27}\mathrm{m}^{-3}$. In all cases $T = 1\mathrm{eV}$.

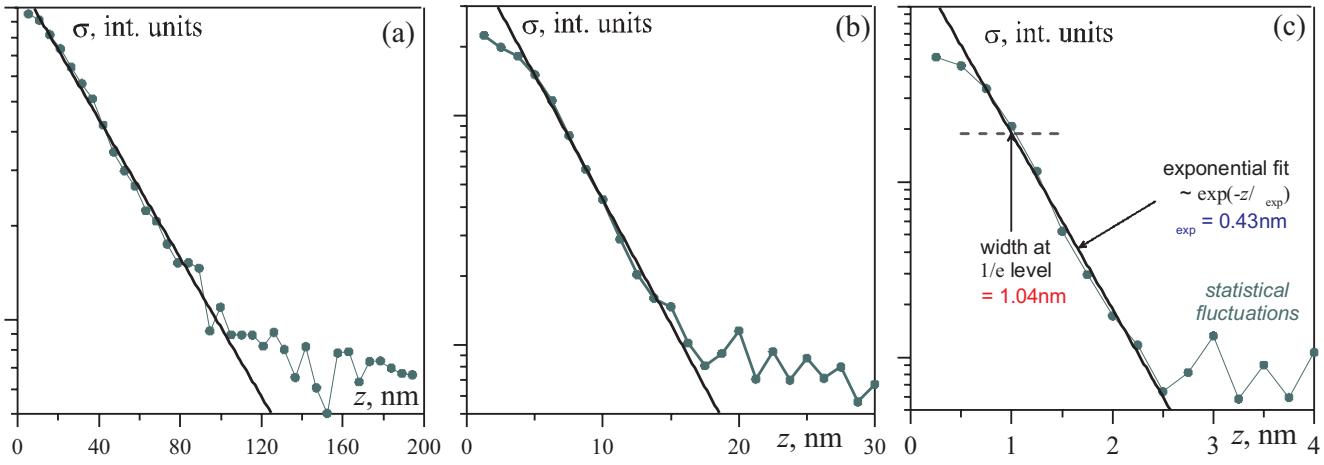

FIG. 7: Distribution of the plasma charge (in internal units) over the longitudinal direction (log-linear plot). Solid line represents the exponential fit, (a) $n_e = 10^{23}\mathrm{m}^{-3}$ (b) $n_e = 10^{25}\mathrm{m}^{-3}$, (c) $n_e = 10^{27}\mathrm{m}^{-3}$. In all cases $T = 1\mathrm{eV}$.

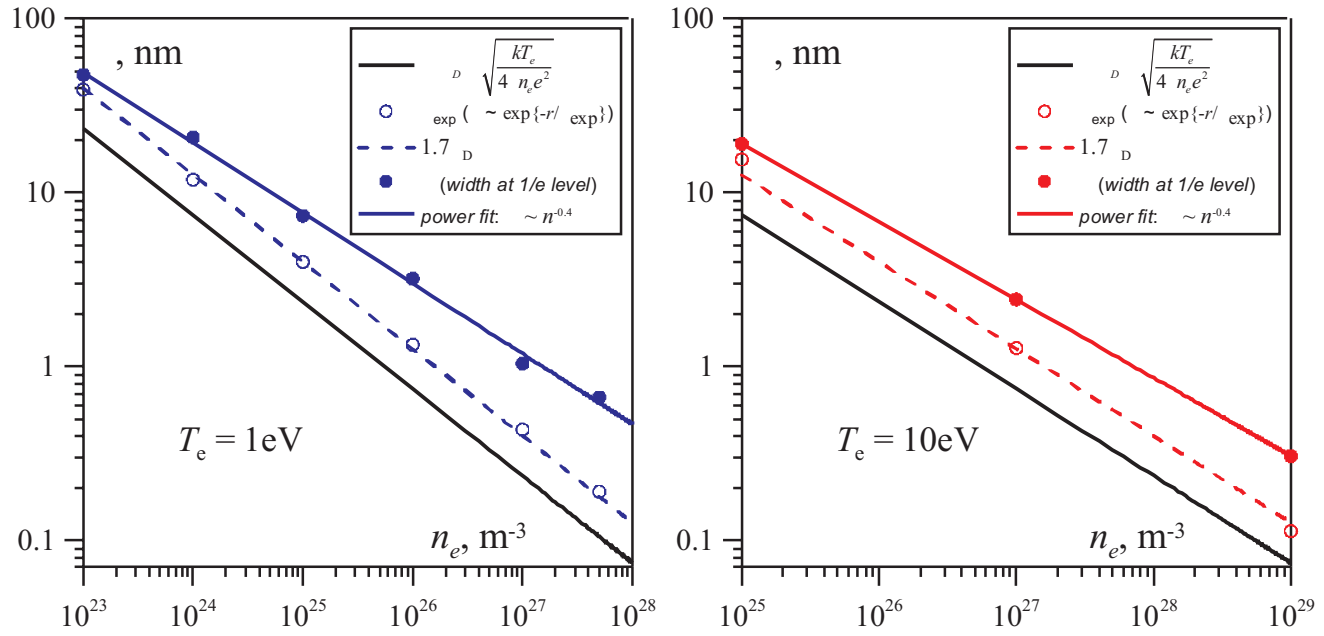

FIG. 8: The Debye length (lower solid line) and the sheath lengths obtained from MD simulations depending on the electron number density. Dashed line is related to the exponential fit (see Fig. 7), higher solid line represents the width λ given by the relation $\sigma(\lambda) = \sigma(0)/e$ where $\sigma(z)$ is the plasma charge profile (Fig. 7). Left figure: $T = 1\mathrm{eV}$, right figure: $T = 10\mathrm{eV}$.

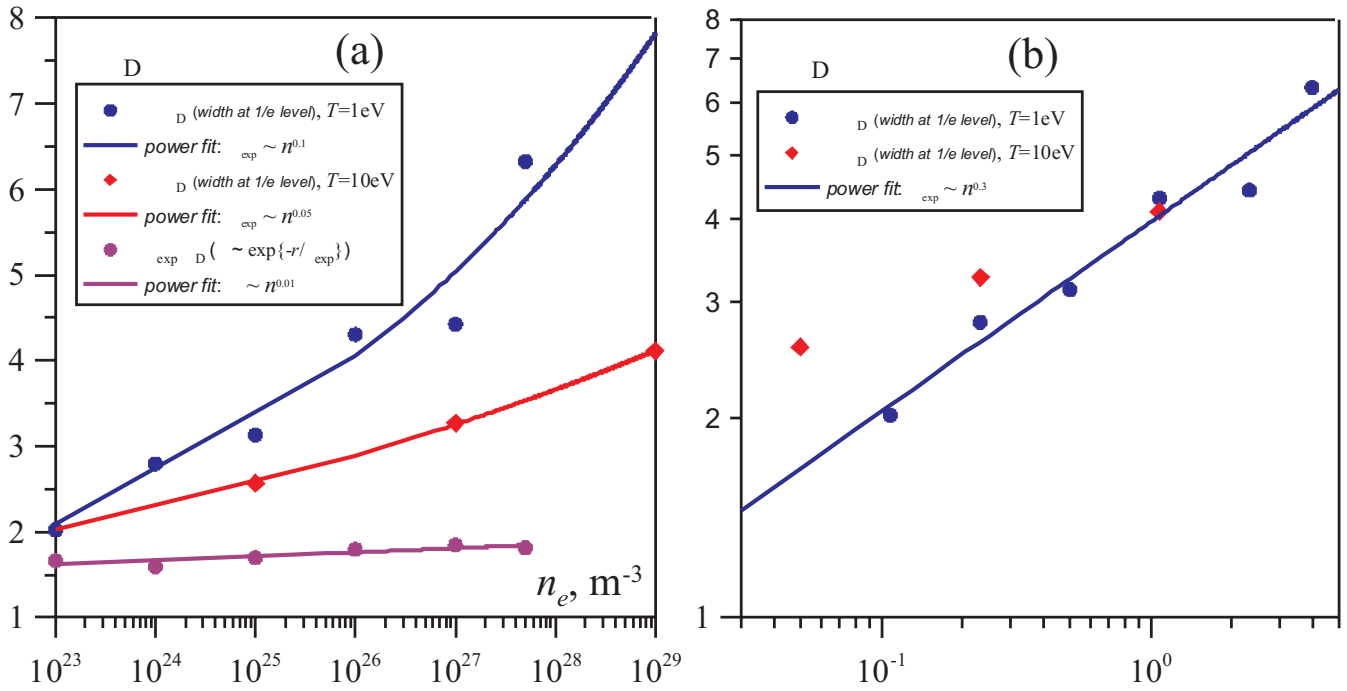

FIG. 9: Dependence of the ratio between the sheath lengths obtained from MD and the Debye length for different temperatures and plasma densities (see the legends). Abscissa axis in plot (b) is the plasma nonideality parameter.

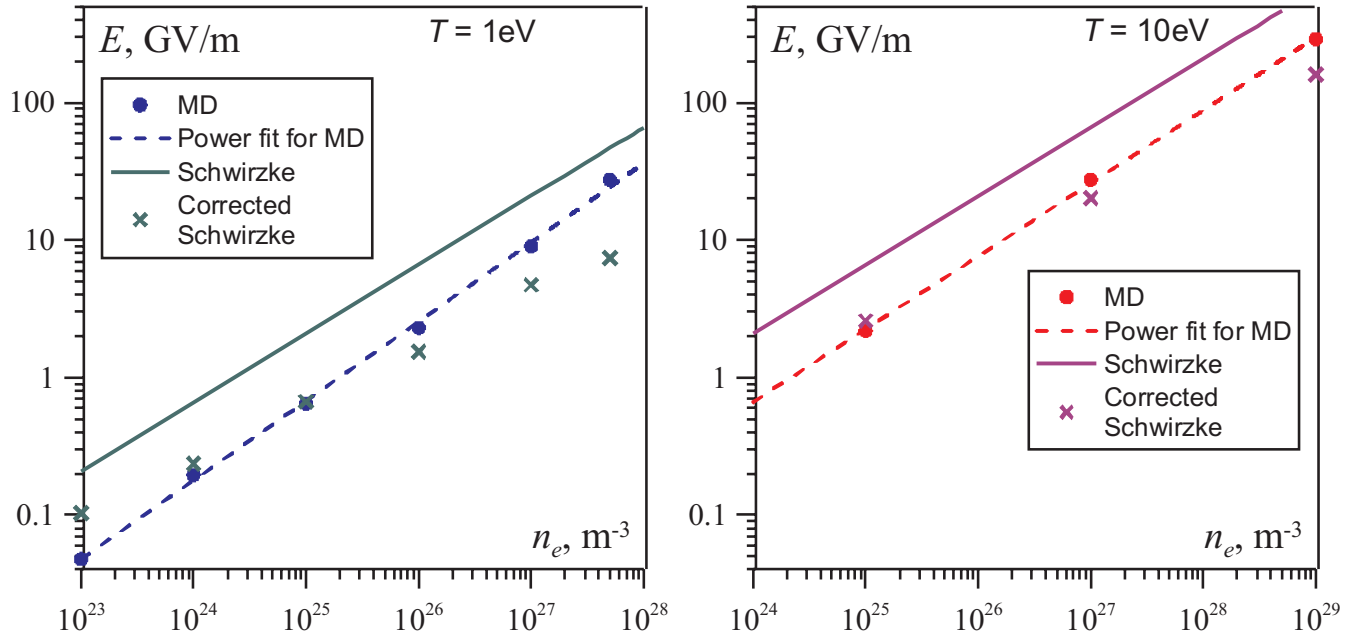

FIG. 10: Dependence of the final surface electric field strength on the electron number density for two values of temperature (shown on prot). MD results are compared with the theoretical estimations from [16]. Crosses correspond to the Eq. (2) from [16] where the Debye length is replaced by the sheath lengths λ obtained from MD (Fig. 8).

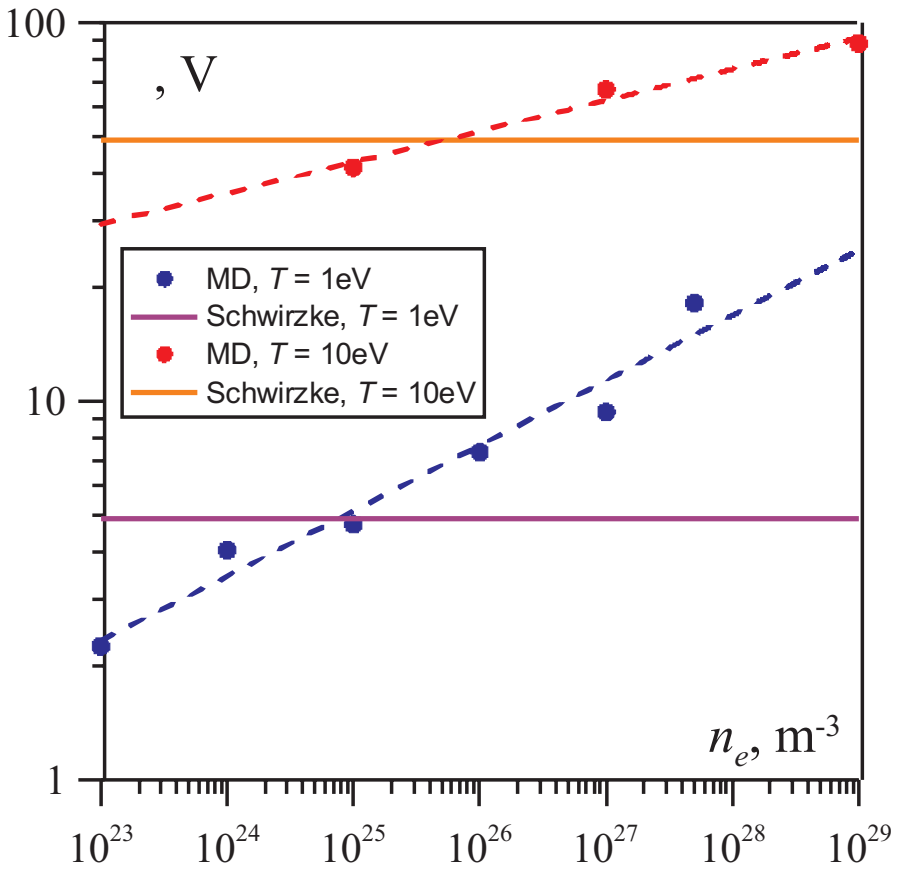

FIG. 11: Plasma potential depending on the density for different temperatures. MD results are compared with the theoretical estimations from [16].

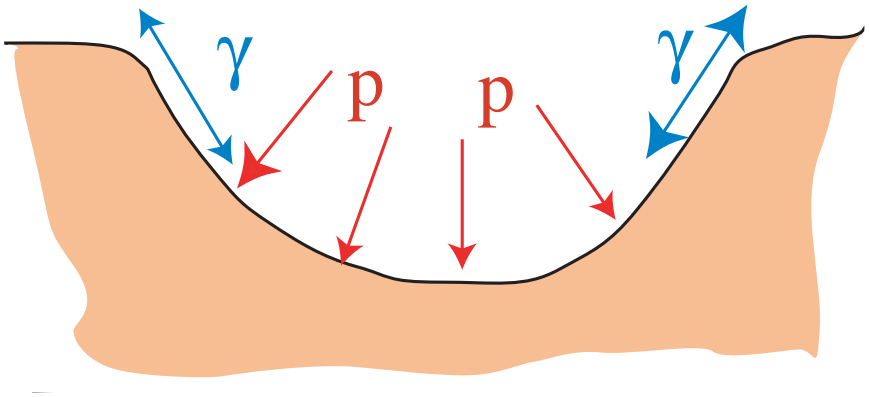

FIG. 12: Plasma pressure (red arrows) is opposed by the surface tension $2\pi\gamma r$.

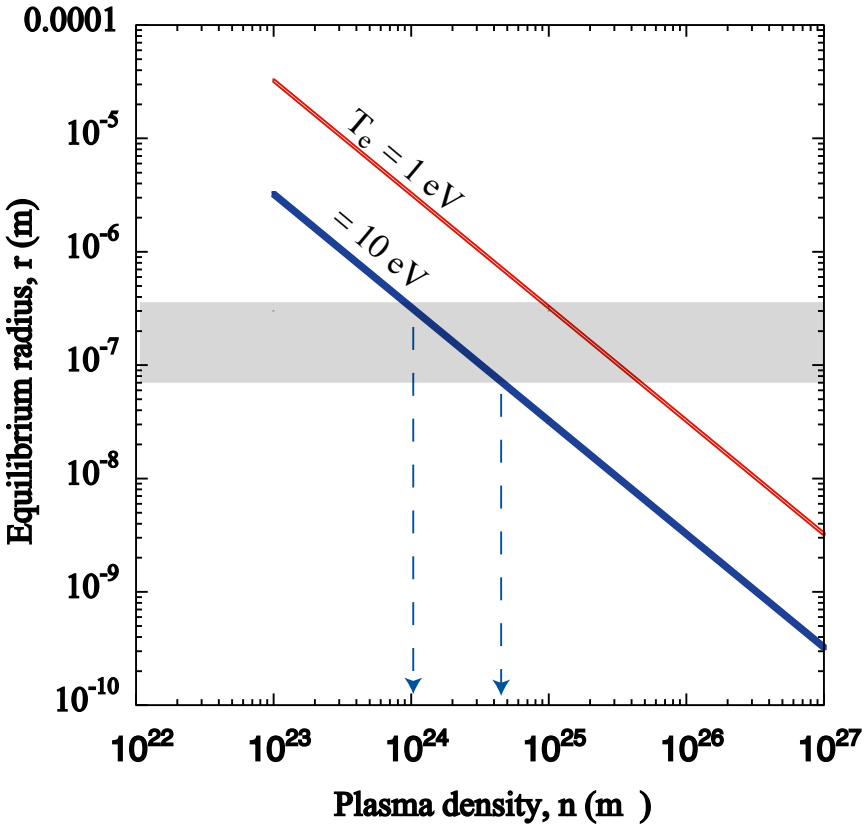

FIG. 13: Equilibrium radius from surface tension and plasma pressure for two electron temperature plasmas compared with dimensions from ref [16].

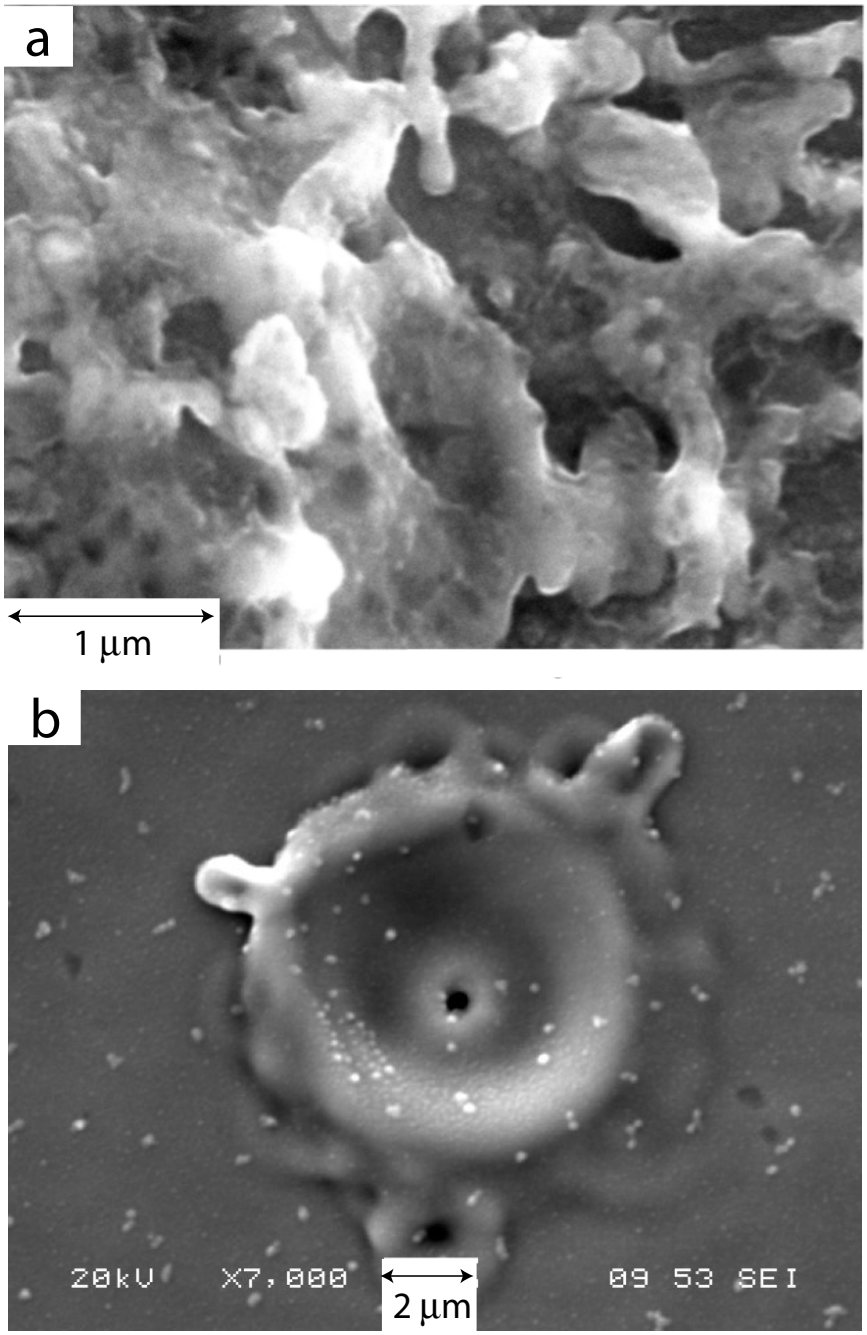

FIG. 14: a) SEM image of unipolar arc tracks from a 201 MHz cavity coupler, showing considerable structure below 1 μm., b) Image of unipolar arc damage from Castano [21].